minerals

MDPI

Article

Lithium Extraction from Dilute Simulated Brines by Membrane-Assisted Liquid-Liquid Extraction Using $[P_{6,6,6,14}][PHOS]$: Li^+/Mg^{2+} Selectivity in an NF90 Nanofiltration Contactor

René Cabezas [1,*], Fernando Mora [1], Ricardo Morales [1], Nicolas Monsalve [1,2], Eduardo Villarroel-Utreras [3] and Luis Pino-Soto [4]

[1] Departamento de Química Ambiental, Facultad de Ciencias, Universidad Católica de la Santísima Concepción, Concepción 4090541, Chile; fmora@qaciencias.ucsc.cl (F.M.); rmorales@qaciencias.ucsc.cl (R.M.); nmonsalve@doctorado.ucsc.cl (N.M.)
[2] Programa de Doctorado en Ciencias con Mención en Biodiversidad y Biorecursos, Facultad de Ciencias, Universidad Católica de la Santísima Concepción, Concepción 4090541, Chile
[3] Grupo en Economía Circular y Tecnologías Ambientales, Facultad de Ingeniería y Negocios, Universidad de Las Américas, Santiago 7500975, Chile; evillarroelu@udla.cl
[4] Departamento de Ingeniería Química, Facultad de Ingeniería, Universidad de Concepción, Concepción 4070386, Chile; luispino@udec.cl
* Correspondence: rene.cabezas@ucsc.cl

Abstract

Selective lithium recovery from dilute brines remains challenging because Li^+ must be separated from competing ions, particularly Mg^{2+}. In this work, a commercial NF90 nanofiltration membrane was used as a non-dispersive interface between a simulated brine and the hydrophobic ionic liquid $[P_{6,6,6,14}][PHOS]$. Individual-salt experiments yielded apparent overall mass transfer coefficients of 638 ± 273, 100.5 ± 19.8, and 10.1 ± 0.7 L m^{-2} h^{-1} for Na^+, Li^+, and Mg^{2+}, respectively. Replacing water with 10% (*v*/*v*) $[P_{6,6,6,14}][PHOS]$ in hexane as the receiving phase increased Li extraction from 18.6 ± 3.0% to 40.9 ± 2.0%. Under direct Li^+/Mg^{2+} competition, selectivities of 2.19 ± 1.10 and 3.83 ± 0.56 were obtained with the diluted and neat ionic liquid receiving phases, respectively. With neat $[P_{6,6,6,14}][PHOS]$, Li extraction reached 40.3%, and 6.0% of the extracted Li was subsequently recovered in pure water under non-optimized conditions. CHNS analysis showed no detectable transfer of organic material derived from the ionic liquid to the aqueous feed. Overall, NF90 was the main source of Li^+/Mg^{2+} transport discrimination, whereas $[P_{6,6,6,14}][PHOS]$ mainly increased Li uptake.

Keywords: lithium extraction; NF90 nanofiltration; hydrophobic ionic liquid; $[P_{6,6,6,14}][PHOS]$; Li^+/Mg^{2+} separation; membrane contactor; simulated brine

Check for updates

Academic Editor: Hyunjung Kim

Received: 19 August 2026
Revised: 8 October 2026
Accepted: 9 October 2026
Published: 11 October 2026

Copyright: © 2026 by the authors. Licensee MDPI, Basel, Switzerland. This article is an open access article distributed under the terms and conditions of the Creative Commons Attribution (CC BY) license.

1. Introduction

Lithium is produced mainly from hard-rock minerals such as spodumene and from continental brines hosted in salt flats or salars [1]. Its growing use in rechargeable batteries, electric vehicles, and stationary energy storage has increased the need for extraction technologies that reduce water consumption, land use, and processing time [1]. Brines are attractive feedstocks because lithium is already dissolved, but selective recovery remains difficult because Li^+ is accompanied by high concentrations of competing salts [2].

Conventional processing of continental brines relies on solar evaporation followed by sequential precipitation to remove calcium, magnesium, boron, sulfates, and other impurities [2–4]. Although this route is well established industrially, it requires large evaporation areas, long residence times, and careful control of the precipitation sequence [2]. In arid regions, these operations have also raised concerns about water balance, landscape alteration, and impacts on salar ecosystems [5].

Salar de Atacama brines contain relatively high lithium concentrations together with substantial amounts of magnesium, sodium, potassium, and calcium [6]. A Mg/Li mass ratio close to 6 has been reported for some Atacama brines [7], illustrating the difficulty of direct Li^+ purification. Conventional Mg^{2+} removal by precipitation or ion exchange can be effective, but it adds unit operations and may lead to lithium losses and solid waste generation [5].

The competing cations are not equally important from a process standpoint. Sodium is highly abundant, but it can be removed upstream by established routes based on halite crystallization followed by fractional crystallization and washing [6]. Magnesium is more difficult to remove and often requires dedicated treatment, with additional reagent consumption and lithium losses through coprecipitation [5]. For this reason, Li^+/Mg^{2+} separation remains a central challenge in brine processing [8,9] and is the main focus of this work. Sodium transport was examined separately in individual-salt experiments.

Li^+/Mg^{2+} separation cannot be explained by the size of the unhydrated ions alone. Both ions are strongly hydrated, but Mg^{2+} has a more stable hydration shell and a larger hydrated size [10]. Separation therefore depends on charge, hydration energy, effective size, electrostatic interactions, solution composition, and affinity for the receiving phase [11,12]. In pressure-driven membrane separation processes, surface charge, pore or transport-domain dimensions, ionic strength, and concentration polarization must also be considered [13,14].

Direct lithium extraction technologies have been developed as alternatives or complements to evaporative concentration. These approaches include lithium-ion sieves [15], ion-imprinted materials [16], ion exchange, liquid–liquid extraction, nanofiltration, electrodialysis, and electrochemical intercalation [17]. Their common goal is to recover lithium from raw or partially conditioned brines while reducing the long processing times associated with solar evaporation. Each route, however, has limitations related to capacity, regeneration, energy demand, material requirements, or interference from other ions [7,18].

Liquid–liquid extraction offers high mass transfer rates and allows the chemical environment of the receiving phase to be adjusted [19]. Direct contact between the aqueous and organic phases, however, can lead to emulsification, phase entrainment, third-phase formation, and gradual extractant loss [20]. These effects complicate phase separation, increase solvent replacement requirements, and may contaminate the treated aqueous stream [18].

Ionic liquids have attracted interest as extraction media because of their negligible vapor pressure, low flammability, high solvation capacity, and structural tunability [21]. In hydrometallurgy, they have been used as extractants, diluents, and functional components of extraction phases. However, their low volatility does not eliminate concerns about viscosity, cost, toxicity, or the transfer of ionic liquid components to the aqueous phase [22,23].

Ionic liquids can also participate directly in the extraction chemistry. Previous work from our group on Re(VII) systems showed that ionic liquid ions can affect extraction stoichiometry, modify the solubility of the extracted complexes, and in some cases partially transfer to the aqueous phase [24,25]. Therefore, both metal affinity and phase confinement must be considered when ionic liquids are used as receiving media.

For lithium, COSMO-RS screening has identified phosphonium ionic liquids as promising candidates for extraction from aqueous solutions. Predicting Mg^{2+} behavior is more complex because several solvation and coordination mechanisms may act simultaneously [26].

Phosphonium ionic liquids have also been evaluated experimentally for conventional lithium solvent extraction [27].

Trihexyl(tetradecyl)phosphonium bis(2,4,4-trimethylpentyl)phosphinate, [$P_{6,6,6,14}$][PHOS], combines a bulky hydrophobic phosphonium cation with a functional phosphinate anion. The long alkyl chains promote water immiscibility, while the oxygen donor sites of the phosphinate group provide a chemically active environment for association with metal species [28]. Thus, the ionic liquid acts as a bifunctional extraction phase rather than as an inert diluent, and its behavior reflects contributions from both ions [29].

The choice of [$P_{6,6,6,14}$][PHOS] was also supported by our previous work with this ionic liquid in membrane processes. It has been used as a receiving phase for vanillin perstraction and for succinic acid separation with cellulose acetate membranes. In those systems, a defined interfacial area was maintained, and transfer of the ionic liquid to the aqueous phase was limited [30,31]. These observations complement thermodynamic screening by providing practical information on phase handling and separation in membrane contactors.

A membrane contactor allows for liquid–liquid extraction without dispersing the two phases and provides a fixed interfacial area for mass transfer [13,32]. The membrane adds mass transfer resistance, but it can also contribute to selectivity. This is especially relevant for nanofiltration membranes, where ion transport is affected by steric exclusion, electrostatic interactions, dielectric effects, and ion hydration [33,34].

Nanofiltration has been widely studied for Li^+/Mg^{2+} separation, mainly under pressure-driven conditions [9,35,36]. Membrane systems containing liquid carriers or ionic liquid phases have also been developed for lithium extraction from model brines [37,38]. These studies show that a membrane can act not only as a physical barrier between the phases but also as a selective barrier coupled to a chemically active receiving phase.

The objective of this work was to evaluate the complementary roles of a commercial NF90 membrane and [$P_{6,6,6,14}$][PHOS] in a non-dispersive Li extraction system. Individual-salt experiments with LiCl, $MgCl_2$, and NaCl were first used to characterize ion transport through NF90. Extraction experiments were then carried out with diluted and neat [$P_{6,6,6,14}$][PHOS]. Finally, competitive Li^+/Mg^{2+} transport was evaluated using an equimass binary simulated brine. This simplified composition was selected to isolate direct Li^+/Mg^{2+} competition rather than to reproduce the complete composition of a specific natural brine.

2. Materials and Methods

2.1. Materials

Lithium chloride (LiCl), magnesium chloride ($MgCl_2$), and sodium chloride (NaCl), all anhydrous and with a stated purity of 99%, were purchased from Merck (Darmstadt, Germany). The hydrophobic ionic liquid trihexyl(tetradecyl)phosphonium bis(2,4,4-trimethylpentyl)phosphinate, [$P_{6,6,6,14}$][PHOS], was supplied by IOLITEC GmbH (Heilbronn, Germany) with a stated assay >90% and a water content <1% by Karl Fischer titration, according to the supplier's certificate of analysis. Hexane (Sigma-Aldrich, St. Louis, MO, USA, ≥95%) was used to prepare a receiving phase containing 10% (*v*/*v*) [$P_{6,6,6,14}$][PHOS]. All aqueous solutions were prepared with ultrapure water. Glucose (Merck, 97.5%–102.5%) was added to the aqueous receiving phase. A commercial FilmTec™ NF90 flat-sheet nanofiltration membrane (DuPont, Wilmington, DE, USA) was used as the selective interface. NF90 is a polypiperazine thin-film composite membrane [39] with a reported molecular weight cut-off of approximately 200 Da [40].

2.2. NF90 Membrane Contactor Cell

Experiments were conducted in a two-compartment glass cell separated by a flat NF90 membrane. The donor and receiving phases were used at a 1:1 volume ratio, with 0.020 L

in each compartment. The effective membrane diameter was 8.1 mm, corresponding to an area of 5.153×10^{-5} m^2, and the total membrane thickness was approximately 100 µm. Before assembly, the NF90 membrane was conditioned in ultrapure water for 24 h and then mounted with its active layer facing the donor phase. Unless otherwise stated, experiments were carried out at 25 °C for 50 min with magnetic stirring in both compartments. A stirring rate of 210 rpm was used with aqueous receivers and with 10% (*v*/*v*) $[P_{6,6,6,14}][PHOS]$ in hexane. Because neat $[P_{6,6,6,14}][PHOS]$ is much more viscous, a stirring rate of 600 rpm was used with this receiving phase. No hydraulic pressure difference was applied across the membrane. All transport conditions were tested in duplicate (n = 2 independent experiments). Figure 1 shows the contact cell, and Figure 2 shows the main structural features of $[P_{6,6,6,14}][PHOS]$.

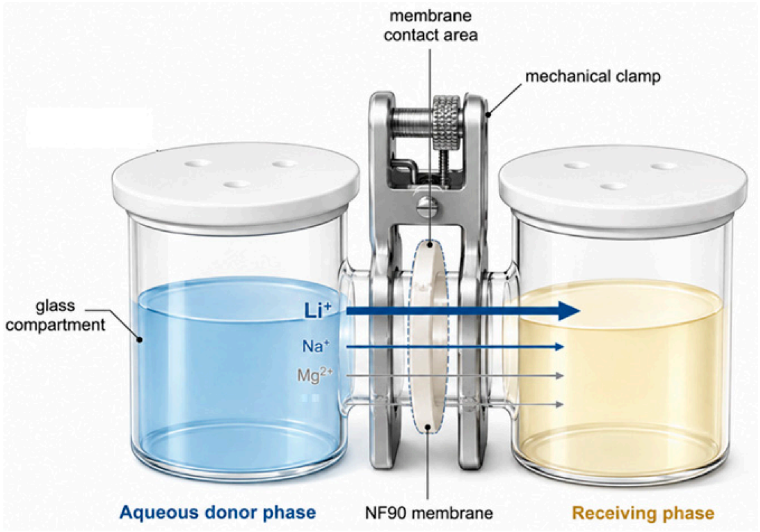


Figure 1. Two-compartment contact cell equipped with a flat NF90 membrane between the aqueous donor phase and the aqueous or extractant receiving phase.

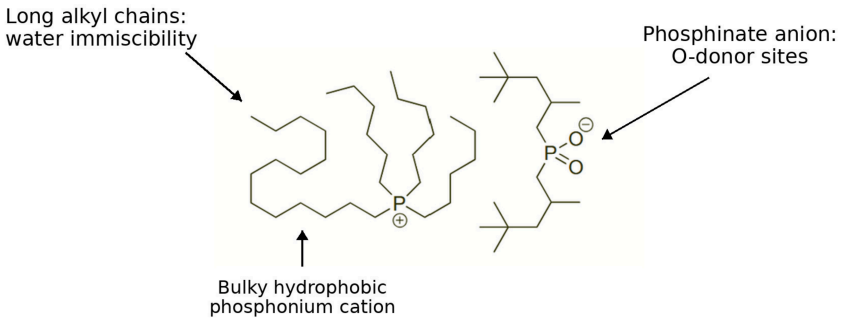


Figure 2. Chemical structure and functional features of $[P_{6,6,6,14}][PHOS]$, highlighting the bulky hydrophobic phosphonium cation, the long alkyl chains responsible for water immiscibility, and the O-donor sites of the phosphinate anion.

2.3. Individual Salt Transport

Transport of LiCl, NaCl, and $MgCl_2$ through NF90 was first evaluated separately. Each donor solution contained 1000 mg L^{-1} of one salt. Concentrations were reported on a salt basis so that all three electrolytes started at the same nominal mass concentration. The receiving compartment contained ultrapure water, with glucose added to reduce the osmotic pressure difference between the two aqueous compartments. Donor concentration was monitored by electrical conductivity using a HANNA Instruments (Woonsocket, RI,

USA) conductivity meter. Five-point calibration curves covering 100–1000 mg L^{-1} were prepared separately for each salt,

$$\kappa = mC + b \quad (1)$$

where κ is the electrical conductivity and C is the salt mass concentration. The calibration equations were $\kappa = 2.0994C + 56.383$ for LiCl ($R^2 = 0.9934$), $\kappa = 1.7710C + 82.171$ for NaCl ($R^2 = 0.9987$), and $\kappa = 1.8870C + 114.7$ for $MgCl_2$ ($R^2 = 0.9992$). The raw calibration data are provided in Figure S1 and Table S1. A separate bilateral LiCl experiment was performed with aqueous donor and receiving phases to follow Li transfer between the two compartments. Li^+, Cl^-, and pH were monitored during this experiment. This experiment was run for 330 min, separately from the standard 50 min transport experiments, to monitor concentration changes in both aqueous compartments and provide an independent assessment of Li^+ and Cl^- transport. Possible salt accumulation in NF90 was evaluated in a separate test by contacting a 10 × 10 cm membrane sample with 100 mL of 1000 mg L^{-1} LiCl for 50 min. The membrane was drained without washing and calcined for 24 h at temperatures up to 600 °C. An identical virgin NF90 sample was calcined in parallel as a blank.

2.4. Extraction with Diluted [$P_{6,6,6,14}$][PHOS]

The individual LiCl and $MgCl_2$ experiments were repeated after replacing the aqueous receiver with 10% (*v*/*v*) [$P_{6,6,6,14}$][PHOS] in hexane while keeping a 1:1 phase volume ratio. The membrane kept the aqueous donor physically separated from the organic receiving phase. Ion transfer therefore required transport from the donor to the membrane, passage through the hydrated NF90 structure, and uptake by the receiving phase. Donor concentration was monitored by conductivity. Li^+ was also measured with an S007 lithium ion-selective electrode (NT Sensors, Vila-seca, Spain) connected to an IMACIMUS ion meter.

2.5. Competitive Extraction from a Simulated Brine

Competition was studied with a binary simulated brine prepared from LiCl and $MgCl_2$. For experiments using 10% (*v*/*v*) [$P_{6,6,6,14}$][PHOS] in hexane, the measured initial concentrations were 526 ± 63 mg L^{-1} Li^+ and 502.1 ± 25.1 mg L^{-1} Mg^{2+}. With neat [$P_{6,6,6,14}$][PHOS], the corresponding values were 553 ± 23 mg L^{-1} Li^+ and 502.1 ± 25.1 mg L^{-1} Mg^{2+}. The equimass composition was selected as a controlled condition for direct Li^+/Mg^{2+} competition. Two receiving phases were evaluated: 10% (*v*/*v*) [$P_{6,6,6,14}$][PHOS] in hexane and neat [$P_{6,6,6,14}$][PHOS], both at a 1:1 phase volume ratio. Li^+ was measured with the ion-selective electrode and Mg^{2+} by atomic absorption spectroscopy. A separate extraction and back-extraction experiment was performed with a LiCl donor and neat [$P_{6,6,6,14}$][PHOS] at a 1:1 phase volume ratio for 120 min. For back-extraction, the loaded ionic liquid was contacted with ultrapure water at an IL:water volume ratio of 1:1 and vortex-mixed at 90 °C for 10 min. The phases were separated while hot. The aqueous phase was then cooled to approximately 4 °C and centrifuged at 1200 rpm for 3 min, and the lower aqueous phase was collected. This cooling and centrifugation step was performed twice to remove residual ionic liquid. A blank was prepared by contacting fresh [$P_{6,6,6,14}$][PHOS] with ultrapure water under the same conditions.

2.6. Analytical Methods

Electrical conductivity was used to determine the concentrations of the individual-salt donor solutions and the LiCl concentrations in the extraction and back-extraction experiment. In the back-extraction experiment, the blank conductivity was subtracted before the LiCl calibration (Equation (1)) was applied. Li^+ was measured with an S007 ion-selective electrode (NT Sensors, Vila-seca, Spain) connected to an IMACIMUS ion meter.

The electrode was calibrated with manufacturer standards at 100, 500, and 1000 mg L^{-1}, and the calibration procedure is shown in Figure S3. Mg^{2+} was determined with an Agilent Technologies 240AA atomic absorption spectrometer (Agilent Technologies Inc., Santa Clara, CA, USA). The Mg^{2+} calibration covered 0–20 mg L^{-1} and followed A = 0.0361C + 0.0235 (R^2 = 0.9961); the calibration data are provided in Figure S2 and Table S2. Chloride was measured with a Hach IntelliCAL™ ISECL181 chloride-selective electrode (Hach Company, Loveland, CO, USA), and pH was recorded in both aqueous compartments. Carbon in the aqueous donor after contact with neat $[P_{6,6,6,14}][PHOS]$ was measured by CHNS elemental analysis using a PerkinElmer PE2400 analyzer (PerkinElmer, Waltham, MA, USA). Selectivity uncertainty was calculated by first-order propagation of the standard deviations of the corresponding apparent mass transfer coefficients.

2.7. Calculation of Transmembrane Flux

The transmembrane mass flux of each species was calculated from the change in donor concentration between the beginning and the end of each experiment:

$$J_i = \left(\frac{V_d}{A}\right)\left(\frac{C_{i,0} - C_{i,f}}{\Delta t}\right) \quad (2)$$

where J_i is the mass flux of species i (g m^{-2} h^{-1}), Vd is the donor volume (L), A is the effective membrane area (m^2), $C_{i,0}$ and C_i,f are the initial and final donor concentrations, and Δt is the experimental time (h). Concentrations were converted from mg L^{-1} to g L^{-1} before calculating the flux to keep Equation (2) dimensionally consistent. With Vd = 0.020 L and A = 5.153 × 10^{-5} m^2, Vd/A = 388.1 L m^{-2}. This finite-volume mass balance is consistent with membrane contactor transport formulations reported previously [13,41]. In the individual-salt experiments, C refers to salt concentration. In the competitive experiments, C refers to the directly measured Li^+ or Mg^{2+} concentration.

The flux was then normalized by the driving force to obtain an apparent overall mass transfer coefficient:

$$K_{i,app} = \frac{J_i}{\Delta C_{i,avg}} \quad (3)$$

where ΔC_i,avg is the time-averaged concentration difference of species i across the membrane, expressed in g L^{-1} for consistency with J_i. It was calculated by trapezoidal integration of the measured concentration difference over the experimental time [13,41].

$$\Delta C_{i,avg} = \frac{1}{t_n \sum_{k=1}^{n} \left(\frac{\Delta C_{i(t_{k-1})} + \Delta C_{i(t_k)}}{2}\right)(t_k - t_{k-1})} \quad (4)$$

For experiments with an aqueous receiving phase, solute accumulation in the receiving compartment was included when calculating ΔC_i,avg. For experiments with an organic receiving phase, the receiver was treated as an effective sink, and ΔC_i,avg was obtained from the time-averaged donor concentration. K_i,app is therefore an apparent overall mass transfer coefficient that includes both membrane and external interfacial resistances. It can vary with solution composition, ionic strength, and operating conditions. Here, it is used as an operational parameter for comparing the evaluated systems rather than as an intrinsic membrane diffusivity.

2.8. Selectivity

The mass-based Li^+/Mg^{2+} selectivity was calculated as the ratio of the corresponding apparent overall mass transfer coefficients:

$$\alpha_{\frac{Li}{Mg}} = \frac{K_{Li,app}}{K_{Mg,app}} \quad (5)$$

Li^+/Na^+ selectivity was calculated in the same way. The selectivity factor is dimensionless, and values greater than one indicate preferential Li^+ transport. Ratios obtained from separate individual-salt experiments are reported as apparent transport selectivities, whereas values obtained from the binary simulated brine describe Li^+/Mg^{2+} separation under direct ion competition [37]. Other nanofiltration studies of Li^+/Mg^{2+} separation, such as Ref. [42], define separation factors from feed and permeate compositions in pressure-driven experiments. These definitions describe the same general concept of Li/Mg discrimination but are not mathematically equivalent to the ratio of apparent mass transfer coefficients used in Equation (5).

3. Results

3.1. Individual Transport of Li^+, Na^+, and Mg^{2+} Through the NF90 Membrane

The first experimental stage examined the contribution of NF90 using an aqueous receiving phase without an extractant. LiCl, NaCl, and $MgCl_2$ were transported from the donor to the receiver at 25 °C. The normalized donor concentration profiles are shown in Figure 3a, and the corresponding transport parameters are summarized in Table 1.

The three electrolytes showed markedly different transport behavior. NaCl was depleted fastest from the donor, decreasing by 42.6 ± 0.4% after 50 min. LiCl showed an intermediate decrease of 18.6 ± 3.0%, whereas $MgCl_2$ decreased by only 2.1 ± 0.1% over the same period. Under concentration-driven conditions, NF90 therefore imposed a much stronger barrier to $MgCl_2$ than to either monovalent electrolyte.

The apparent overall mass transfer coefficients followed the sequence $K_{Na,app}$ = 638.1 ± 273.1 > $K_{Li,app}$ = 100.5 ± 19.8 > $K_{Mg,app}$ = 10.1 ± 0.7 L m^{-2} h^{-1}. In the bilateral LiCl experiment, donor Li^+ decreased from 128.6 to 110.6 mg L^{-1} after 30 min, while Cl^- in the receiving phase increased from 0.10 to 92.13 mg L^{-1}. Based on the 1:1 stoichiometry of LiCl, the 18.0 mg L^{-1} decrease in Li^+ corresponds to 92.0 mg L^{-1} Cl^- [18.0 × (35.45/6.94)], in close agreement with the independently measured increase in the receiver. Donor pH remained close to 6.90 throughout the experiment, and Li^+ accumulation was also observed in the receiving phase. In the membrane retention control, the additional inorganic residue associated with NF90 corresponded to approximately 0.031 mg after normalization to the effective membrane area. This represented less than 1% of the mass transferred in the LiCl/water experiment. The complete bilateral Li^+ and pH data are provided in Table S3, the chloride data in Table S4, and the membrane retention control in Figure S4 and Table S5.

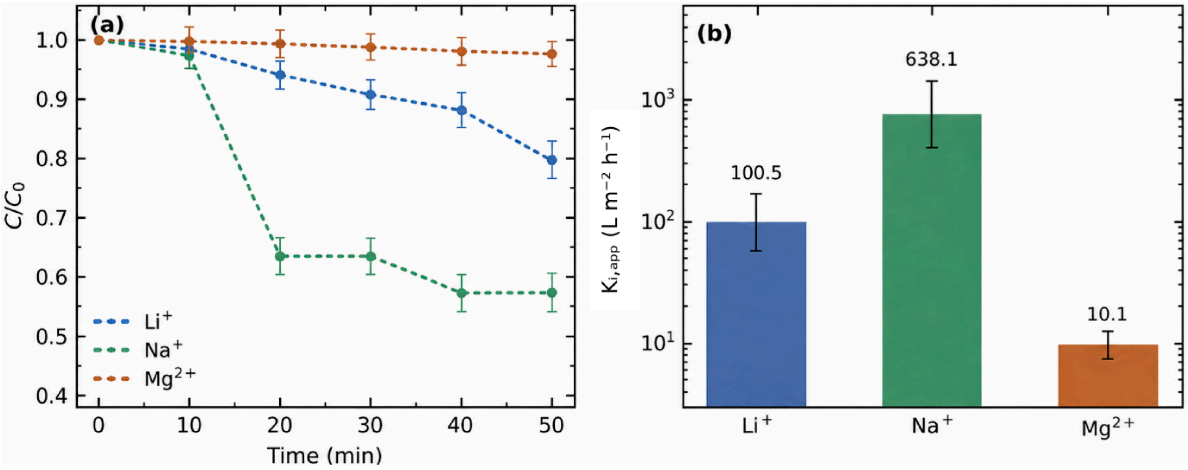


Figure 3. Individual-salt transport through NF90 with an aqueous receiving phase at 25 °C. (**a**) Normalized donor concentration profiles. (**b**) Apparent overall mass transfer coefficients (K_i,app) shown on a logarithmic scale.

Table 1. Transport of LiCl, NaCl, and $MgCl_2$ through NF90 with an aqueous receiving phase. 25 °C, 1:1 volume ratio.

Salt	C_0 (mg L^{-1})	C_f (mg L^{-1})	Decrease (%)	Mass Transferred (mg)	J (g m^{-2} h^{-1})	$K_{i,app}$ (L m^{-2} h^{-1})
LiCl	1022.0	831.5 ± 30.3	18.6 ± 3.0	3.811 ± 0.606	88.74 ± 14.12	100.5 ± 19.8
NaCl	1015.2	582.9 ± 3.6	42.6 ± 0.4	8.645 ± 0.072	201.32 ± 1.68	638.1 ± 273.1
$MgCl_2$	994.3	973.1 ± 1.5	2.1 ± 0.1	0.424 ± 0.030	9.87 ± 0.69	10.1 ± 0.7

3.2. Effect of the Receiving Phase on Lithium Transport

After the transport behavior of NF90 was established with an aqueous receiver, the receiver was replaced with 10% (*v*/*v*) $[P_{6,6,6,14}][PHOS]$ in hexane. Figure 4 and Table 2 compare LiCl and $MgCl_2$ transport with the corresponding experiments using water as the receiver. Hexane was used only as a diluent. In conventional solvent extraction, hydrated metal ions are strongly hydrophilic and generally require coordination with an extractant to form hydrophobic species that can transfer to the organic phase [43]. Therefore, appreciable Li^+ or Mg^{2+} extraction by hexane alone is not expected in the absence of a coordinating extractant. In this system, $[P_{6,6,6,14}][PHOS]$ is the chemically active component of the receiving phase.

Table 2. Effect of receiving-phase composition on LiCl and $MgCl_2$ transport through NF90. 25 °C, 1:1 volume ratio.

System	C_0 (mg L^{-1})	C_f (mg L^{-1})	Decrease (%)	J (g m^{-2} h^{-1})	$K_{i,app}$ (L m^{-2} h^{-1})
LiCl/water	1022.0	831.5 ± 30.3	18.6 ± 3.0	88.74 ± 14.12	100.5 ± 19.8
LiCl/hexane + 10% (*v*/*v*) $[P_{6,6,6,14}][PHOS]$	1022.0	604.3 ± 30.2	40.9 ± 2.0	194.56 ± 9.73	254.8 ± 12.7
$MgCl_2$/water	994.3	973.1 ± 1.5	2.1 ± 0.1	9.87 ± 0.69	10.1 ± 0.7
$MgCl_2$/hexane + 10% (*v*/*v*) $[P_{6,6,6,14}][PHOS]$	994.3	920.7 ± 46.0	7.4 ± 0.4	34.31 ± 1.72	35.6 ± 1.8

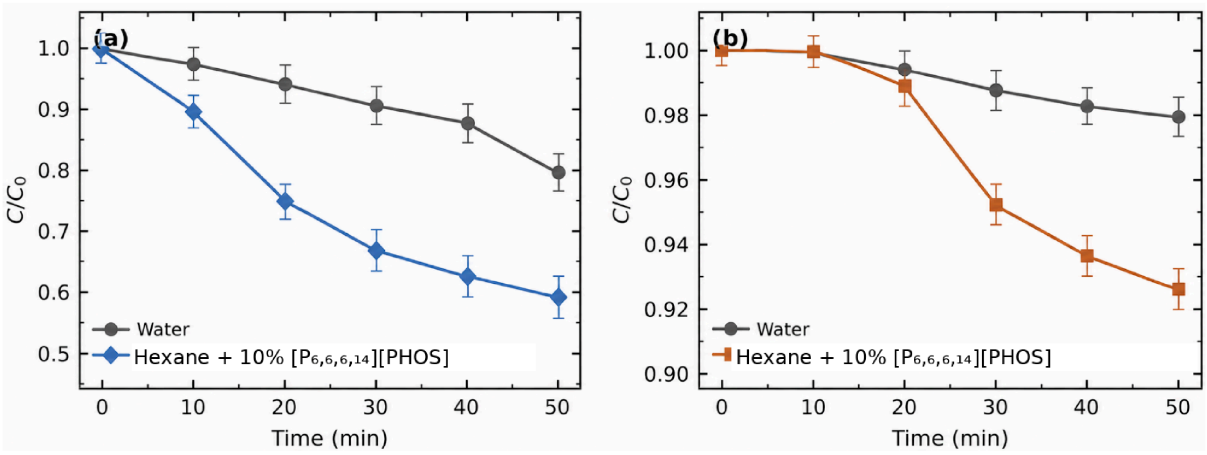


Figure 4. Effect of receiving-phase composition on transport through NF90 at 25 °C. (**a**) Li^+ and (**b**) Mg^{2+}.

Replacing water with the ionic liquid receiving phase increased LiCl donor depletion from 18.6 ± 3.0% to 40.9 ± 2.0% and raised $K_{Li,app}$ from 100.5 ± 19.8 to 254.8 ± 12.7 L m^{-2} h^{-1}. The mass of LiCl transferred over 50 min increased from 3.81 ± 0.61 to 8.36 ± 0.42 mg. This increase is consistent with Li uptake by the phosphinate-containing receiving phase, which maintains a larger driving force than water at the membrane/receiver interface.

$MgCl_2$ transport also increased with the ionic liquid receiving phase. Donor depletion rose from 2.1 ± 0.1% to 7.4 ± 0.4%, and $K_{Mg,app}$ increased from 10.1 ± 0.7 to 35.6 ± 1.8 L m^{-2} h^{-1}. The relative increase was larger for Mg than for Li, indicating that $[P_{6,6,6,14}][PHOS]$ enhances receiving-phase uptake but is not the main source of Li/Mg discrimination. In the separate experiment with neat IL, the donor LiCl concentration decreased from 1011 to 603 mg L^{-1} after 120 min, corresponding to 40.3% extraction. After back-extraction at 90 °C, the aqueous phase had a conductivity of 220.3 µS cm^{-1}, compared with 112.8 µS cm^{-1} for the blank. The blank-corrected value of 107.5 µS cm^{-1} corresponds to 24.35 mg L^{-1} LiCl. Because both steps were carried out at a 1:1 phase ratio, this concentration represents 6.0% of the LiCl transferred to the ionic liquid (407.7 mg L^{-1}). Hot water therefore stripped only a small fraction of the Li retained by $[P_{6,6,6,14}][PHOS]$. CHNS analysis of the aqueous donor after contact with neat $[P_{6,6,6,14}][PHOS]$ gave 0.01%–0.02% C, similar to the 0.02% C measured in the LiCl aqueous reference. No enrichment in organic material derived from the ionic liquid was detected under the conditions evaluated. The complete CHNS results and the extraction/back-extraction calculation are provided in Tables S6 and S7, respectively.

3.3. Competitive Li^+/Mg^{2+} Transport from a Simulated Brine

Competitive experiments were carried out with an equimass binary simulated brine prepared from LiCl and $MgCl_2$. Table 3 reports the initial concentrations for each receiving phase. With 10% (*v*/*v*) $[P_{6,6,6,14}][PHOS]$ in hexane, the initial concentrations were 526 ± 63 mg L^{-1} Li^+ and 502.1 ± 25.1 mg L^{-1} Mg^{2+}. With neat $[P_{6,6,6,14}][PHOS]$, they were 553 ± 23 mg L^{-1} Li^+ and 502.1 ± 25.1 mg L^{-1} Mg^{2+}. Figure 5 and Table 3 summarize the concentration profiles and competitive selectivities for both receiving phases.

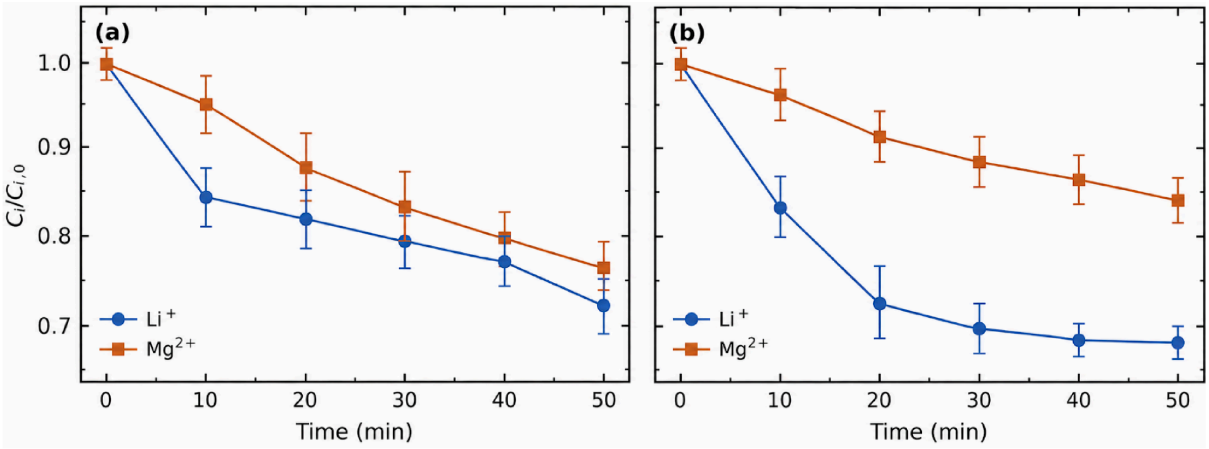


Figure 5. Competitive transport of Li^+ and Mg^{2+} from the binary simulated brine at 25 °C using (**a**) 10% $[P_{6,6,6,14}][PHOS]$ in hexane and (**b**) neat $[P_{6,6,6,14}][PHOS]$ as receiving phases.

Table 3. Competitive Li^+ and Mg^{2+} transport from the binary simulated brine with $[P_{6,6,6,14}][PHOS]$-based receiving phases.

Receiving Phase	$C_{0,Li}$	$C_{f,Li}$	Li^+ Decrease (%)	$C_{0,Mg}$	$C_{f,Mg}$	Mg^{2+} Decrease (%)	$\alpha_{Li/Mg}$
Hexane + 10% IL	526 ± 63	396 ± 23	24.5 ± 4.6	502.1 ± 25.1	434.4 ± 18.9	13.5 ± 3.8	2.19 ± 1.10
Neat $[P_{6,6,6,14}][PHOS]$	553 ± 23	410 ± 12	25.8 ± 5.3	502.1 ± 25.1	460.6 ± 15.5	8.3 ± 3.1	3.83 ± 0.56

Li^+ donor depletion was greater than Mg^{2+} depletion in both receiving phases. With 10% $[P_{6,6,6,14}][PHOS]$ in hexane, Li^+ and Mg^{2+} decreased by 24.5 ± 4.6% and 13.5 ± 3.8%,

respectively. With neat [$P_{6,6,6,14}$][PHOS], the corresponding decreases were 25.8 ± 5.3% and 8.3 ± 3.1%. The two formulations therefore differed mainly in Mg^{2+} transport, since Li^+ transfer was similar in both cases. Dilution with hexane lowers the viscosity of the receiving phase and can reduce liquid-side resistance, but it also lowers the local ionic liquid concentration and changes the interfacial coordination environment. Neat [$P_{6,6,6,14}$][PHOS], in contrast, is much more viscous, which can increase liquid-side resistance even at the higher stirring rate used. The similar Li^+ depletion obtained with the two formulations suggests that these opposing effects partly compensate under the conditions tested, while Mg^{2+} transport is more sensitive to the receiving-phase formulation.

The concentration profiles show rapid Li^+ transfer at the beginning of the experiment, followed by a gradual decrease in the transfer rate. In this finite-volume contactor, donor depletion reduces the concentration gradient as the experiment proceeds. At the same time, solute accumulation near the membrane/receiver interface and in the receiving phase can increase the importance of liquid-side and interfacial resistances. This effect is expected to be stronger for the more viscous neat ionic liquid. Mg^{2+} remains strongly restricted by NF90, so changes in the receiving phase affect Mg^{2+} and Li^+ differently. The higher competitive selectivity obtained with neat [$P_{6,6,6,14}$][PHOS] (3.83 ± 0.56 versus 2.19 ± 1.10) is therefore mainly associated with lower Mg^{2+} transfer rather than with higher Li^+ extraction.

3.4. Individual-Salt and Competitive Selectivity

Apparent individual-salt selectivity was calculated from K_i,app values obtained in separate salt experiments. Competitive selectivity was calculated from experiments in which Li^+ and Mg^{2+} were present together. This comparison shows how separation changes when direct ion competition and the higher ionic strength of the binary brine are introduced. The results are summarized in Table 4 and Figure 6.

Table 4. Apparent individual-salt and competitive Li^+/Mg^{2+} selectivity of the NF90/[$P_{6,6,6,14}$][PHOS] system at 25 °C.

System	Type	$K_{Li,app}$ (L m^{-2} h^{-1})	$K_{Mg,app}$ (L m^{-2} h^{-1})	$\alpha_{Li/Mg}$ (-)
NF90/water	Individual-salt	100.5 ± 19.8	10.1 ± 0.7	9.95 ± 0.50
NF90/hexane + 10% IL	Individual-salt	254.8 ± 12.7	35.6 ± 1.8	7.15 ± 0.36
NF90/hexane + 10% IL	Competitive	135.8 ± 27.1	67.3 ± 21.5	2.19 ± 1.10
NF90/neat [$P_{6,6,6,14}$][PHOS]	Competitive	149.9 ± 38.6	40.3 ± 16.0	3.83 ± 0.56

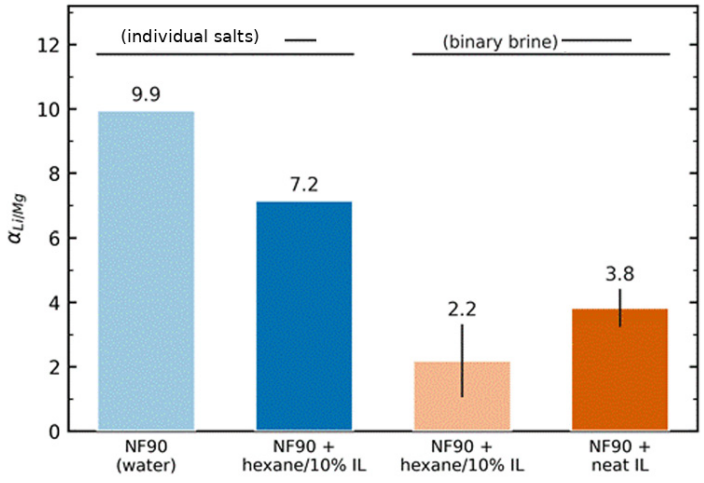


Figure 6. Apparent individual-salt selectivity obtained from separate salt experiments and competitive selectivity obtained from the binary Li^+/Mg^{2+} simulated brine.

With water as the receiving phase, NF90 gave an apparent individual-salt Li^+/Mg^{2+} selectivity of 9.95 ± 0.50. This value decreased to 7.15 ± 0.36 with 10% $[P_{6,6,6,14}][PHOS]$ in hexane because Mg transport increased proportionally more than Li transport. Under direct competition, selectivity decreased further to 2.19 ± 1.10 with the diluted receiving phase and to 3.83 ± 0.56 with neat $[P_{6,6,6,14}][PHOS]$. These results indicate that NF90 is the main source of Li/Mg discrimination, whereas the ionic liquid mainly increases transport capacity.

4. Discussion

4.1. Transport Mechanisms Through the NF90 Membrane

The individual-salt experiments were carried out at similar initial mass concentrations, allowing direct comparison of donor depletion and flux. The much lower transport of $MgCl_2$ compared with LiCl and NaCl is consistent with the combined effects of ion hydration, steric restriction, dielectric exclusion, and electrostatic partitioning in NF90 [11,33,34]. Mg^{2+} has a larger hydration shell and a higher charge density than the monovalent cations, which makes its entry into the selective layer less favorable both energetically and sterically. The observed trend therefore reflects the behavior of the complete NF90 contactor and should not be attributed to a single exclusion mechanism.

Electrostatic effects also depend on ionic strength. NF90 is commonly reported to be negatively charged near neutral pH, but charge-based discrimination decreases as electrolyte concentration increases because electrostatic interactions are screened [14,44]. This effect may contribute to the lower Li^+/Mg^{2+} discrimination observed in the competitive brine. However, the present experiments were not designed to separate Donnan, dielectric, and steric contributions.

The sequence $K_{Na,app} > K_{Li,app} > K_{Mg,app}$ is also consistent with differences in cation hydration. Li^+ has a larger hydrated radius than Na^+ despite its smaller crystal radius [10], in agreement with its lower transport coefficient. Mg^{2+} combines a larger hydrated size with a divalent charge and is therefore much more strongly restricted. The apparent overall coefficients include both membrane and external boundary-layer resistances and should not be interpreted as intrinsic molecular diffusivities of the NF90 selective layer.

The bilateral LiCl experiment provides independent support for this interpretation. As described in Section 3.1, the expected chloride transfer was calculated from the measured Li^+ decrease using the 1:1 LiCl stoichiometry and the molar mass ratio MCl/MLi. The calculated value of 92.0 mg L^{-1} Cl^- agrees closely with the measured increase of 92.03 mg L^{-1} in the receiver, supporting coupled counterion transport. Donor pH remained nearly constant, indicating that the concentration change was not accompanied by a major bulk acid-base shift. The membrane residue test also showed that accumulation within or on NF90 was too small to explain the measured donor depletion.

The relatively large dispersion of $K_{Na,app}$ (638.1 ± 273.1 L m^{-2} h^{-1}) can be explained by the way this parameter is calculated. NaCl showed the fastest donor depletion, so the time-averaged transmembrane concentration difference became relatively small. Because $K_{i,app}$ is obtained by dividing the flux by this driving force, small run-to-run changes in the denominator produce a larger relative variation in the calculated coefficient. In contrast, the directly measured NaCl donor depletion showed little variation (42.6 ± 0.4%). $K_{Na,app}$ is therefore treated here as an apparent operational coefficient rather than an intrinsic membrane property.

4.2. Origin of the Selectivity Loss Under Competitive Conditions

The lower Li^+/Mg^{2+} selectivity under competitive conditions can be explained by several effects acting together. First, Li^+ and Mg^{2+} share the same phosphinate-containing receiving phase and may compete for favorable environments at the interface and in the

receiving phase. Second, the higher ionic strength of the binary brine increases electrostatic screening in NF90, which can reduce monovalent/divalent discrimination [14,45]. Third, ionic fluxes are coupled by electroneutrality, as supported by the chloride measurements in the bilateral LiCl experiment. These effects are consistent with the observed decrease in selectivity, although their individual contributions cannot be quantified from the present data.

The change is also evident from the apparent transport coefficients. With 10% [$P_{6,6,6,14}$] [PHOS] in hexane, $K_{Li,app}$ decreased from 254.8 ± 12.7 L m^{-2} h^{-1} in the individual-salt Li experiment to 135.8 ± 27.1 L m^{-2} h^{-1} under competition, while $K_{Mg,app}$ increased from 35.6 ± 1.8 to 67.3 ± 21.5 L m^{-2} h^{-1}. The lower competitive selectivity therefore reflects both lower Li transport and higher Mg transport. Further improvement will require maintaining the Mg^{2+} restriction provided by the membrane while preserving sufficient Li uptake in the receiving phase.

Sodium must also be considered for process applications. In the individual-salt experiments, NF90 transported Na^+ faster than Li^+, giving $\alpha_{Li/Na} = 0.16$. The present configuration should therefore not be interpreted as a single-step purification process for untreated raw brine. It would be better suited for use after upstream operations have reduced the sodium content, or as part of a broader treatment sequence in which Li/Mg separation is the main role of this membrane contactor [3,6,46].

4.3. Implications for Brine Processing and Study Limitations

The equimass binary simulated brine was selected as a controlled Li^+/Mg^{2+} competition matrix rather than as a reconstruction of one specific salar composition. Natural brines cover a wide range of Li and Mg concentrations, and the Mg/Li ratio also changes during solar concentration as different salts precipitate [3,6,7]. The competitive selectivities measured here should therefore be interpreted only for the composition tested and should not be extrapolated directly to a fixed number of industrial cascade stages.

Comparison with other membrane-based lithium separation systems helps place the present results in context (Table 5). Studies on polymer inclusion membranes containing P507-TBP have reported Li/Mg separation factors of 10.2 in binary feeds and 21.8 in synthetic multicomponent brines [37]. Ionic liquid-based polymer inclusion membranes have shown a Li/Mg selectivity of approximately 2.2 under their specific feed conditions [38], while a recent hollow-fiber supported ionic liquid membrane contactor reached separation factors of up to 30.8 at high Mg/Li ratios [47]. These values cannot be compared directly because membrane architecture, carrier chemistry, feed composition, phase ratio, and driving force differ among studies. The present system instead combines a commercial NF90 membrane as the selective barrier with a phosphonium ionic liquid receiving phase.

Recent concentration-gradient dialysis studies with highly charged membranes have also shown that selective partitioning and uphill Mg^{2+} transport can produce strong Li/Mg discrimination without a hydraulic pressure gradient [48]. These results further illustrate the importance of membrane partitioning in concentration-driven separations. The main limitations of the present NF90/[$P_{6,6,6,14}$][PHOS] system are the simplified binary feed, the short duration of the standard transport experiments, the absence of competitive Li/Na measurements, the lack of direct quantitative Li analysis in the ionic liquid phase, and the low Li back-extraction obtained with hot water. In addition, membrane surface charge was not measured under the experimental conditions used here. The discussion of Donnan screening therefore relies on NF90 behavior reported in the literature rather than on a direct zeta-potential measurement in this study.

Table 5. Representative membrane-based Li/Mg separation systems using liquid carriers or ionic liquid receiving phases. Values are reported as presented in the cited studies and are not directly comparable because operating conditions differ.

Membrane Configuration	Carrier/ Receiving Phase	Feed Condition	Driving Principle	Li/Mg Selectivity	Ref.
CTA-based polymer inclusion membrane	TBP-$[C_4mim][NTf_2]$	7.2 mM LiCl + 2.06 mM $MgCl_2$	Carrier-mediated transport	2.2	[38]
CTA/P507-TBP polymer inclusion membrane	P507-TBP	0.1 M LiCl + 4.0 M $MgCl_2$	Carrier-mediated transport	10.2 (21.8 in synthetic brine)	[37]
14-crown-4-functionalized polyimide hollow-fiber SILM	TBP + $NaNTf_2$	High-Mg/Li model brine; Mg/Li up to 35	Supported ionic-liquid membrane contactor	up to 30.8	[47]
NF90 flat-sheet contactor (this work)	10% or neat $[P_{6,6,6,14}][PHOS]$	Equimass Li^+/Mg^{2+} simulated brine	Concentration-gradient transport; $\Delta P = 0$	2.19/3.83	This work

4.4. Future Development of the NF90/[P$_{6,6,6,14}$][PHOS] Contactor

Future work should first focus on a quantitative description of the mass transfer mechanism. The concentration profiles measured in both compartments provide a basis for models that include donor and receiver boundary layers, membrane resistance, the concentration-dependentdriving force, and ionic coupling. Experiments that vary stirring rate, temperature, initial concentration, membrane area, and phase volume ratio would help separate the contributions of external mass transfer, membrane transport, and receiving-phase uptake, and would provide a stronger basis for scale-up.

A second priority is direct quantification of Li in $[P_{6,6,6,14}][PHOS]$. Matrix-matched calibration for atomic absorption spectroscopy, or another elemental technique suitable for this matrix, is needed to determine Li loading in the ionic liquid and close the Li mass balance independently of donor depletion.

The back-extraction experiment showed that water at 90 °C recovered only a small fraction of the Li captured by the ionic liquid. Future work should therefore evaluate the composition of the stripping solution, the phase ratio, the contact time, and multistage contact to increase Li recovery while limiting dilution. Once Li is transferred to an aqueous stream, conventional precipitation routes such as Li_2CO_3 formation can be considered after suitable concentration and impurity control.

Other recovery routes for the Li-loaded ionic liquid can also be considered. The electrochemical window of ionic liquids makes electrochemical Li recovery an option worth investigating, provided that Li speciation and redox behavior in $[P_{6,6,6,14}][PHOS]$ are first established. Another possibility is to couple the loaded ionic liquid with electrodialysis or another electromembrane process so that a second ion-selective barrier contributes to Li recovery. These options are still exploratory and should be compared in terms of recovery, selectivity, energy demand, and ionic liquid regeneration before a process route is selected.

5. Conclusions

NF90 acted as a selective non-dispersive barrier between aqueous Li-containing solutions and $[P_{6,6,6,14}][PHOS]$. In the individual-salt experiments, transport followed the order $K_{Na,app} > K_{Li,app} > K_{Mg,app}$ and gave an apparent Li^+/Mg^{2+} selectivity of 9.95 ± 0.50, indicating that the membrane provides the main Li/Mg discrimination. Replacing water

with an ionic liquid receiving phase increased Li transfer, but Mg transport increased proportionally more. Thus, $[P_{6,6,6,14}][PHOS]$ mainly increased receiving-phase uptake rather than providing the dominant selectivity.

Under direct Li^+/Mg^{2+} competition, selectivity decreased to 2.19 ± 1.10 with 10% $[P_{6,6,6,14}][PHOS]$ in hexane and to 3.83 ± 0.56 with neat $[P_{6,6,6,14}][PHOS]$. In a separate 120 min experiment with neat IL, Li extraction reached 40.3%, but back-extraction with water at 90 °C recovered only 6.0% of the extracted Li. CHNS analysis showed no detectable enrichment of the aqueous feed in organic material derived from the ionic liquid. Overall, the system combines Li/Mg discrimination provided by the membrane with a hydrophobic receiving phase that remains physically separated from the aqueous feed, although more effective stripping conditions are needed to recover Li from the loaded ionic liquid.

Supplementary Materials: The following supporting information can be downloaded at: https://www.mdpi.com/article/10.3390/min16101038/s1, Figure S1: Conductivity calibration curves for LiCl, NaCl, and $MgCl_2$; Figure S2: Mg^{2+} calibration by flame atomic absorption spectroscopy; Figure S3: IMACIMUS calibration interface for the S007 Li^+ ion-selective electrode; Figure S4: Bilateral LiCl transport and NF90 membrane-retention control; Table S1: Raw conductivity calibration data for LiCl, NaCl, and $MgCl_2$; Table S2: Mg^{2+} calibration data for atomic absorption spectroscopy; Table S3: Bilateral LiCl experiment, Li^+ concentration and pH in donor and receiving phases; Table S4: Chloride concentrations measured during the bilateral LiCl experiment; Table S5: NF90 membrane-retention control and normalization to the effective contact area; Table S6: CHNS elemental analysis of aqueous LiCl solutions used to assess possible transfer of ionic-liquid-derived organic material; Table S7: Extraction with neat $[P_{6,6,6,14}][PHOS]$ and back-extraction with water at 90 °C.

Author Contributions: Conceptualization, R.C. and L.P.-S.; Methodology, R.C., R.M., L.P.-S. and E.V.-U.; Formal Analysis, R.C., N.M. and R.M.; Investigation, N.M., R.M. and F.M.; Visualization, R.C., R.M. and E.V.-U.; Writing—Original Draft Preparation, R.C. and N.M.; Writing—Review and Editing, R.C. and E.V.-U.; Supervision, R.C.; Project Administration, R.C.; Funding Acquisition, R.C. and L.P.-S. All authors have read and agreed to the published version of the manuscript.

Funding: This research was funded by the Chilean National Agency for Research and Development (ANID) through FONDECYT Regular Project No. 1241812, FOVI 250157, FONDEF IT25I0111, ANID-Centros Consorcio Hídrico COTH2O CTI250001, and FONDECYT Iniciación Project No. 11261111.

Data Availability Statement: The original contributions presented in this study are included in the article and its Supplementary Materials. Further inquiries can be directed to the corresponding author.

Acknowledgments: Nicolas Monsalve acknowledges support from the ANID Doctoral Scholarship Program, Grant No. 21263145.

Conflicts of Interest: The authors declare no conflicts of interest.

References

1. Grosjean, C.; Herrera Miranda, P.; Perrin, M.; Poggi, P. Assessment of world lithium resources and consequences of their geographic distribution on the expected development of the electric vehicle industry. *Renew. Sustain. Energy Rev.* **2012**, *16*, 1735–1744. [CrossRef]
2. Flexer, V.; Baspineiro, C.F.; Galli, C.I. Lithium recovery from brines: A vital raw material for green energies with a potential environmental impact in its mining and processing. *Sci. Total Environ.* **2018**, *639*, 1188–1204. [CrossRef] [PubMed]
3. Ogawa, Y.; Koibuchi, H.; Suto, K.; Inoue, C. Effects of the chemical compositions of Salars de Uyuni and Atacama brines on lithium concentration during evaporation. *Resour. Geol.* **2014**, *64*, 91–101. [CrossRef]
4. Neira, A.; Gálvez, E.; Mura, M.; Galleguillos-Madrid, F.M.; Picazo Rodríguez, N.G.; Saldana, M.; Leiva, W.; Toro, N.; Castillo, J. Technologies for Boron Removal from Lithium-Rich Brines: A Review. *Minerals* **2026**, *16*, 807. [CrossRef]
5. Vera, M.L.; Torres, W.R.; Galli, C.I.; Chagnes, A.; Flexer, V. Environmental impact of direct lithium extraction from brines. *Nat. Rev. Earth Environ.* **2023**, *4*, 149–165. [CrossRef]
6. Torres, D.; Pérez, K.; Galleguillos Madrid, F.M.; Leiva, W.H.; Gálvez, E.; Salinas-Rodríguez, E.; Gallegos, S.; Jamett, I.; Castillo, J.; Saldana, M.; et al. Salar de Atacama lithium and potassium productive process. *Metals* **2024**, *14*, 1095. [CrossRef]

7. Murphy, O.; Haji, M.N. A review of technologies for direct lithium extraction from low Li+ concentration aqueous solutions. *Front. Chem. Eng.* **2022**, *4*, 1008680. [CrossRef]
8. Li, T.; Liu, Y.; Srinivasakannan, C.; Jiang, X.; Zhang, N.; Zhou, G.; Yin, S.; Li, S.; Zhang, L. Comparison of the Mg^{2+}–Li+ separation of different nanofiltration membranes. *Membranes* **2023**, *13*, 753. [CrossRef] [PubMed]
9. Zhang, L.; Hu, M.; He, B.; Pei, H.; Li, X.; Matsuyama, H. A review of the nanofiltration membrane for magnesium and lithium separation from salt-lake brine. *Sep. Purif. Technol.* **2025**, *354*, 129169. [CrossRef]
10. Nightingale, E.R. Phenomenological theory of ion solvation. Effective radii of hydrated ions. *J. Phys. Chem.* **1959**, *63*, 1381–1387. [CrossRef]
11. Bowen, W.R.; Welfoot, J.S. Modelling the performance of membrane nanofiltration—Critical assessment and model development. *Chem. Eng. Sci.* **2002**, *57*, 1121–1137. [CrossRef]
12. Gao, L.; Wang, H.; Zhang, Y.; Wang, M. Nanofiltration membrane characterization and application: Extracting lithium in lepidolite leaching solution. *Membranes* **2020**, *10*, 178. [CrossRef] [PubMed]
13. Gabelman, A.; Hwang, S.-T. Hollow fiber membrane contactors. *J. Membr. Sci.* **1999**, *159*, 61–106. [CrossRef]
14. Roth, R.S.; Birnhack, L.; Avidar, M.; Hjelvik, E.A.; Straub, A.P.; Epsztein, R. Effect of solution ions on the charge and performance of nanofiltration membranes. *npj Clean Water* **2024**, *7*, 25. [CrossRef]
15. Gao, Y.-Y.; Sun, Y.; Chen, L.; Tan, Y.; Fan, R.; Hai, C.; Zhang, H. Progress of research in titanium-based lithium-ion sieves for the extraction of lithium from salt lake brine. *ACS Omega* **2025**, *10*, 11643–11657. [CrossRef] [PubMed]
16. Zhi, K.; Duan, J.; Zhang, J.; Huang, L.; Guo, L.; Wang, L. Progress and prospect of ion imprinting technology in targeted extraction of lithium. *Polymers* **2024**, *16*, 833. [CrossRef] [PubMed]
17. Park, J.; Lee, J.; Shim, I.-T.; Kim, E.; Nam, S.-H.; Koo, J.-W.; Hwang, T.-M. Electrochemical direct lithium extraction: A review of electrodialysis and capacitive deionization technologies. *Resources* **2025**, *14*, 27. [CrossRef]
18. Swain, B. Recovery and recycling of lithium: A review. *Sep. Purif. Technol.* **2017**, *172*, 388–403. [CrossRef]
19. Meng, X.; Zou, X.; Jiang, Y.; Zhou, H.; Zhao, J.; Zhang, S.; Zhang, J. Selective recovery lithium from mother liquor via solvent extraction: A review on extractants, mechanisms, and efficiency. *Separations* **2026**, *13*, 55. [CrossRef]
20. Rodríguez Varela, R.; Chagnes, A.; Forsberg, K. Third-phase formation in rare earth element extraction with D2EHPA: Key factors and impact on liquid membrane extraction performance. *Membranes* **2025**, *15*, 188. [CrossRef] [PubMed]
21. Yudaev, P.A.; Chistyakov, E.M. Ionic liquids as components of systems for metal extraction. *ChemEngineering* **2022**, *6*, 6. [CrossRef]
22. Gonçalves, A.R.P.; Paredes, X.; Cristino, A.F.; Santos, F.J.V.; Queirós, C.S.G.P. Ionic liquids—A review of their toxicity to living organisms. *Int. J. Mol. Sci.* **2021**, *22*, 5612. [CrossRef] [PubMed]
23. Quijada-Maldonado, E.; Olea, F.; Sepúlveda, R.; Castillo, J.; Cabezas, R.; Merlet, G.; Romero, J. Possibilities and challenges for ionic liquids in hydrometallurgy. *Sep. Purif. Technol.* **2020**, *251*, 117289. [CrossRef]
24. Quijada-Maldonado, E.; Allain, A.; Pérez, B.; Merlet, G.; Cabezas, R.; Tapia, R.; Romero, J. Selective liquid–liquid extraction of molybdenum(VI) and rhenium(VII) from a synthetic pregnant leach solution: Comparison between extractants and diluents. *Miner. Eng.* **2020**, *145*, 106060. [CrossRef]
25. Villarroel, E.; Olea, F.; Araya-López, C.; Gajardo, J.; Merlet, G.; Cabezas, R.; Romero, J.; Quijada-Maldonado, E. Diluent effects in the solvent extraction of rhenium(VII) with amine extractants in [Tf2N]-based ionic liquids: Experimental and COSMO-RS analysis. *J. Mol. Liq.* **2022**, *346*, 117091. [CrossRef]
26. Olea, F.; Durán, G.; Díaz, G.; Villarroel, E.; Araya-López, C.; Cabezas, R.; Merlet, G.; Romero, J.; Quijada-Maldonado, E. Ionic liquids for the selective solvent extraction of lithium from aqueous solutions: A theoretical selection using COSMO-RS. *Minerals* **2022**, *12*, 190. [CrossRef]
27. Shi, C.; Jing, Y.; Xiao, J.; Wang, X.; Jia, Y. Liquid–liquid extraction of lithium using novel phosphonium ionic liquid as an extractant. *Hydrometallurgy* **2017**, *169*, 314–320. [CrossRef]
28. Zhou, H.; Ye, Y.; Tan, Y.; Zhu, K.; Liu, X.; Tian, H.; Guo, Q.; Wang, L.; Zhao, S.; Liu, Y. Supported liquid membranes based on bifunctional ionic liquids for selective recovery of gallium. *Membranes* **2022**, *12*, 376. [CrossRef] [PubMed]
29. Malki, M.; Mitiche, L.; Sahmoune, A.; Fontàs, C. New insights on Y, La, Nd, and Sm extraction with bifunctional ionic liquid Cyphos IL 104 incorporated in a polymer inclusion membrane. *Membranes* **2024**, *14*, 182. [CrossRef] [PubMed]
30. Olea, F.; Merlet, G.; Araya-López, C.; Cabezas, R.; Villarroel, E.; Quijada-Maldonado, E.; Romero, J. Separation of vanillin by perstraction using hydrophobic ionic liquids as extractant phase: Analysis of mass transfer and screening of ILs via COSMO-RS. *Sep. Purif. Technol.* **2021**, *274*, 119008. [CrossRef]
31. Zurob, E.; Quijada-Maldonado, E.; Castro-Muñoz, R.; Romero, J.; Plaza, A.; Cabezas, R. Development of an asymmetric cellulose acetate–ionic liquid $P_{6,6,6,14}$[PHOS] gel membrane for the perstraction of succinic acid from a model fermentation solution of Yarrowia lipolytica. *Sep. Purif. Technol.* **2025**, *354*, 129199. [CrossRef]
32. Olea, F.; Ulloa, L.; Bringas, E.; Urzúa-Ahumada, J.; Abejón, R.; Romero, J.; Quijada-Maldonado, E. Selective separation of La(III) and Ce(III) using hollow fiber membranes: Influence of pH and extractant systems. *Minerals* **2025**, *15*, 167. [CrossRef]
33. Yaroshchuk, A.E. Dielectric exclusion of ions from membranes. *Adv. Colloid Interface Sci.* **2000**, *85*, 193–230. [CrossRef] [PubMed]

34. Zeng, X.; Meng, C.; Xu, Z.; Li, X.; Zhu, H.; Li, G. Recent advances on the positively-charged nanofiltration membranes for Mg2+/Li+ separation through interfacial polymerization. *Nanomaterials* **2025**, *15*, 967. [CrossRef] [PubMed]
35. Liu, L.; Lin, S.; Xu, X.; Wan, Y.; Song, W.; Luo, J. Preference of negatively charged membranes in magnesium and lithium separation by nanofiltration. *Nat. Commun.* **2025**, *16*, 5731. [CrossRef] [PubMed]
36. Somrani, A.; Hamzaoui, A.H.; Pontié, M. Study on lithium separation from salt lake brines by nanofiltration (NF) and low pressure reverse osmosis (LPRO). *Desalination* **2013**, *317*, 184–192. [CrossRef]
37. Zeng, X.; Xu, L.; Deng, T.; Zhang, C.; Xu, W.; Zhang, W. Polymer inclusion membranes with P507–TBP carriers for lithium extraction from brines. *Membranes* **2022**, *12*, 839. [CrossRef] [PubMed]
38. Xu, L.; Zeng, X.; He, Q.; Deng, T.; Zhang, C.; Zhang, W. Stable ionic liquid-based polymer inclusion membranes for lithium and magnesium separation. *Sep. Purif. Technol.* **2022**, *288*, 120626. [CrossRef]
39. DuPont. FilmTec™ NF90 Element: Nanofiltration Elements for Commercial Systems. Product Data Sheet, Form No. 45-D01520-en, Rev. 8. April 2026. Available online: https://www.dupont.com/content/dam/water/amer/us/en/water/public/documents/en/NF-FilmTec-NF90-PDS-45-D01520-en.pdf (accessed on 8 October 2026).
40. Ramdani, A.; Deratani, A.; Taleb, S.; Drouiche, N.; Lounici, H. Performance of NF90 and NF270 commercial nanofiltration membranes in the defluoridation of Algerian brackish water. *Desalin. Water Treat.* **2021**, *212*, 286–296. [CrossRef]
41. Ho, C.-D.; Chang, H.; Tu, J.-W.; Lim, J.-W.; Chiou, C.-P.; Chen, Y.-J. Theoretical and experimental studies of CO2 absorption in double-unit flat-plate membrane contactors. *Membranes* **2022**, *12*, 370. [CrossRef] [PubMed]
42. Hubach, T.; Pillath, M.; Knaup, C.; Schlüter, S.; Held, C. Li^+ separation from multi-ionic mixtures by nanofiltration membranes: Experiments and modeling. *Modelling* **2023**, *4*, 408–425. [CrossRef]
43. Li, Z.; Dewulf, B.; Binnemans, K. Nonaqueous Solvent Extraction for Enhanced Metal Separations: Concept, Systems, and Mechanisms. *Ind. Eng. Chem. Res.* **2021**, *60*, 17285–17302. [CrossRef] [PubMed]
44. Saavedra, A.; Valdés, H.; Velásquez, J.; Hernández, S. Comparative analysis of Donnan steric partitioning pore model and dielectric exclusion applied to the fractionation of aqueous saline solutions through nanofiltration. *ChemEngineering* **2024**, *8*, 39. [CrossRef]
45. Li, R.; Zheng, Y.; Zhang, X.; Tan, M.; Wang, J.; Tian, G. Enhanced lithium recovery from salt-lake brines via advanced nanofiltration membranes: Polymeric structure–sieving performance relationships. *Polymers* **2025**, *17*, 1440. [CrossRef] [PubMed]
46. Warnock, S.J.; Sujanani, R.; Zofchak, E.S.; Zhao, S.; Dilenschneider, T.J.; Hanson, K.G.; Mukherjee, S.; Ganesan, V.; Freeman, B.D.; Abu-Omar, M.M.; et al. Engineering Li/Na selectivity in 12-crown-4-functionalized polymer membranes. *Proc. Natl. Acad. Sci. USA* **2021**, *118*, e2022197118. [CrossRef] [PubMed]
47. Dong, B.; Hua, J.; He, J.; Du, J.; Xiao, J.; Li, J. A hollow fiber supported ionic liquid membrane contactor for continuous extraction of lithium from high magnesium/lithium ratio brine. *Water Res.* **2025**, *279*, 123451. [CrossRef] [PubMed]
48. Santiago-Pagán, L.; Patel, H.; Kitto, D.; Bentley, A.; Kamcev, J. Selective partitioning and uphill transport enable effective Li/Mg ion separation by negatively charged membranes. *Nat. Chem. Eng.* **2025**, *2*, 747–759. [CrossRef]

Disclaimer/Publisher's Note: The statements, opinions and data contained in all publications are solely those of the individual author(s) and contributor(s) and not of MDPI and/or the editor(s). MDPI and/or the editor(s) disclaim responsibility for any injury to people or property resulting from any ideas, methods, instructions or products referred to in the content.